

1 Fast charging for electric vehicles applications: numerical
2 optimization of a multi-stage charging protocol for lithium-ion
3 battery and impact on cycle life

4 Romain Mathieu^{a,*}, Olivier Briat^a, Philippe Gyan^b, Jean-Michel Vinassa^a

5 ^aUniv. Bordeaux, CNRS, Bordeaux INP, IMS, UMR 5218, F-33400, Talence, France

6 ^bRenault, FR TCR LAB 012, Technocentre de Guyancourt, 1 avenue du golf, 78084, Guyancourt, France

7 **Abstract**

8 One challenge of fast charging for electric vehicles is the potential degradation caused by high
9 charge currents on the battery. This article focuses on the numerical optimization of fast charging
10 protocols and on their impact on battery cycle life. An optimization problem is formulated to
11 define the parameters of a multi-stage of constant current charging protocol. The problem is
12 based on a strongly coupled electro-thermal model and is developed to achieve fast charging
13 while taking aging into account in an implicit manner.

14 The proposed method is used to define optimized protocols in different operating conditions
15 in terms of ambient temperature, charging time, and charged capacity. Experimental aging tests
16 are then conducted to investigate their impact on the cycle life of a lithium-ion cell. Optimized
17 protocols are compared with fast charging reference protocols in similar operating conditions.
18 The results show that the optimized protocols can reduce the charging time and/or the degradation
19 compared to the reference protocols. This indicates that there exist opportunities for significantly
20 higher currents to reduce battery charging time while still maintaining a long cycle life.

21 *Key words:* electric vehicles, fast charge, numerical optimization, aging, lithium-ion battery,
22 temperature dependency

23 **1. Introduction**

24 Fast charging of lithium-ion batteries is an important step towards the adoption of electric
25 vehicles. The deployment of very high power charging systems is underway in several regions

*Corresponding author: romain_mathieu@gmail.com

Preprint submitted to the *Journal of Energy Storage*

April 12, 2021

26 thanks to the coordination of both public and private actors [1]. This current deployment mo-
27 tivates many research works on the battery side, to make lithium-ion batteries accept higher
28 charging power and effectively reduce charging times [2, 3]. This paper focuses on the issue of
29 optimized fast charging protocols.

30 The charging protocol controls current, voltage, and/or power during the charging stage of
31 batteries [4]. In general, the goal of optimized fast charging protocols is to find the best com-
32 promise between a low charging time, a high energy charged, and a high durability [5], which
33 are contradictory objectives. In particular, durability has to be carefully considered because high
34 charge currents rates are often considered as a factor of aging acceleration [5–7]. The reason
35 comes from several aging mechanisms such as lithium plating [8], solid electrolyte interphase
36 (SEI) growth [9] and mechanical degradation [10, 11]. These mechanisms depend strongly on
37 battery states such as state-of-charge (SOC), temperature and state-of-health (SOH). Thus, pa-
38 rameters of charging protocols should vary depending on the operating conditions.

39 Therefore, optimized fast charging protocols seek to design the charge current or power pro-
40 file with the highest rates possible that minimizes aging. Two key questions are raised. The first
41 one concerns the choice of a charging protocol, which determines the charge current or power
42 profile. The second one concerns the definition of its parameters, which decide the value of
43 charge current or power. While considering the choice of a protocol, many have been proposed
44 in the literature such as constant current-constant voltage (CC-CV) protocols [5, 12], multi-stage
45 of constant current (MSCC) protocols [13, 14], pulse-charging protocols [13, 15], and uncon-
46 strained protocols or protocols that follow a defined trajectory [15–17]. While considering the
47 definition of optimized charging protocols parameters, they are two main approaches in the liter-
48 ature: experimental and numerical. The experimental approach seeks to observe an experimental
49 criterion whose value limits the charge current or power. It involves methods such as three-
50 electrode tests [18–20], mechanical activity monitoring [21], voltage relaxation tests [22], or
51 design-of-experiments [15, 23, 24]. The numerical approach is based on a mathematical model
52 of battery behavior and on numerical optimization methods. This paper considers the numerical
53 optimization approach, because it is well suited for the intrinsic compromise that fast charging
54 protocols have to offer. It also has the ability to rapidly define protocols for many operating
55 conditions.

56 Several contributions to the definition of charging protocols by numerical optimization have

57 been published in the literature [14, 16, 17, 25–28]. They differ by the underlying model used,
58 the optimization problem and the realization of experimental aging tests or lack thereof. The
59 aforementioned articles bring notable improvements; however, in our perspective, there remains
60 several issues that limit their potential for defining fast charging protocols in real electric vehicle
61 applications. The main issue concerns the impact of these protocols on the cycle life of lithium-
62 ion batteries. Some studies did not realize experimental aging tests [25–27]. Therefore, the
63 impact of such optimized protocols on aging was not validated experimentally. Lin *et al.* realized
64 such experimental tests; however, they did not provide detailed information on the cell used [28].
65 Thus, the results cannot be interpreted comprehensively because the electrode materials and
66 energy density of the cell are not known, although they strongly influence aging [29]. Three
67 studies provided more information on aging. Perez *et al.* observed that the optimized protocol
68 increased the degradation compared to a reference CC-CV protocol with a similar charging time
69 [17]. Guo *et al.* witnessed that the optimized protocol allowed to decrease the degradation
70 compared to a reference CC-CV protocol [16]. Yet, the charging time of the reference protocol
71 was significantly inferior, which skews the comparison. Zhang *et al.* observed that the optimized
72 protocol caused a similar degradation compared to a reference CC-CV protocol, for a charging
73 time divided by two [14]. Nevertheless, the charging time of the optimized protocol is still
74 superior to one hour, which is high for the high power cell that is investigated and cannot be
75 considered as fast charging [5, 30]. Consequently, in our opinion, there is a need for additional
76 experimental aging data to demonstrate the applicability of such optimized protocols for electric
77 vehicles.

78 The objective of our study is to experimentally investigate the possibility to define protocols,
79 that limit the impact of fast charging on battery lifetime, by numerical optimization. To fulfill
80 this objective, this paper reports on a numerical optimization method that we developed and fur-
81 ther used to define fast charging protocols. Then, the degradation that these protocols induce
82 is experimentally compared on a high energy cell with reference CC-CV protocols, that were
83 investigated in one of our previous studies [31], and under similar operating conditions. Section
84 2 details the numerical background and the optimization problem developed to define the param-
85 eters of a MSCC charging protocol. Section 3 presents the experimental aging tests achieved to
86 verify the impact on cycle life of the optimized protocols. Finally, Section 4 reports and discusses
87 the degradation results by comparing the optimized protocols with reference CC-CV protocols.

88 **2. Optimization problem and numerical results**

89 This section first justifies the choice of the protocol and presents the underlying model used
 90 for simulating battery behavior. Then, it describes the formulation of the optimization problem
 91 and shows examples of numerical results.

92 *2.1. Multi-step of constant current (MSCC) charging protocol*

93 We choose to optimize the charge based on a multi-stage of constant current protocol (MSCC).
 94 Figure 1 illustrates its principle. The charging process is separated in n stages of constant cur-
 95 rent (CC) [I_1, I_2, \dots, I_n], which are combined with n voltage thresholds [U_1, U_2, \dots, U_n], which
 96 control the end of each CC stage. The end of stages can also be controlled by SOC thresholds
 97 [$SOC_1, SOC_2, \dots, SOC_n$]. In this article, voltage thresholds are preferred as they do not need to
 98 be adapted to a decreasing capacity unlike SOC thresholds.

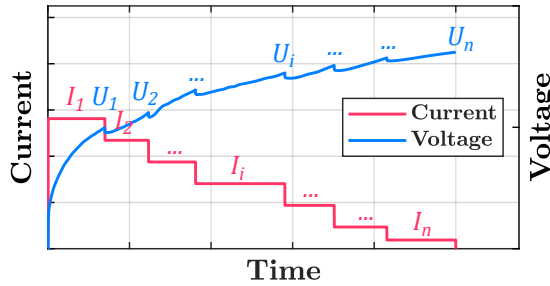


Figure 1: Theoretical illustration of current (red) and voltage (blue) profiles vs. time during a MSCC protocol with current stages delimited by voltage thresholds.

99 The MSCC protocol can be used with progressively increasing U_i thresholds such as illus-
 100 trated in Figure 1. In this case, its principle is to apply different charge current rates depending on
 101 the SOC range. Proceeding this way, the MSCC protocol allows a finer tuning than the CC-CV
 102 protocol [32]. In particular, it can decrease the current in the last stages of the charging process
 103 to avoid aging mechanisms that are amplified by high SOC, such as lithium plating [18, 21]. An
 104 unconstrained protocol or a protocol following a current trajectory can also provide this advan-
 105 tage. However, the definition of the MSCC protocol parameters is simplified and is well suited
 106 to a numerical optimization problem. Moreover, the straightforward structure of this protocol

107 promotes its implementation into electric vehicle charging systems. For all these reasons, we
 108 expect the MSCC protocol to provide good performances for fast charging optimization.

109 2.2. Coupled electro-thermal model

110 To represent the battery behavior during charge, an electrical model is coupled with ther-
 111 mal dynamics. The framework of the coupled electro-thermal model used is based on existing
 112 works in the literature [33–35]. This subsection thus briefly describes its main equations and its
 113 parameterization methods.

114 The electrical model is an equivalent circuit model. It computes the evolution of the cell
 115 voltage U (in volts) in relation to the applied current I (in amperes, a positive current convention
 116 in charge is considered) during time t . The cell voltage is expressed with three terms as

$$U = U_{oc} + \eta_{\Omega} + \sum_{j=1}^n \eta_j. \quad (1)$$

117 The first term is the open-circuit voltage U_{oc} . It is mainly a function of the state-of-charge
 118 SOC . The SOC is computed according to Eq. 2, where SOC_{ini} is the initial SOC and Q_c is the
 119 cell capacity (in Ah). As the coulombic efficiency of lithium-ion cells is generally high (superior
 120 to 99%), it can be ignored in Eq. 2 without significant errors in SOC estimation because the
 121 model is only used in this study to simulate a single charge. The second term is the ohmic
 122 overvoltage η_{Ω} . Its value is computed by Eq. 3, where R_{Ω} is a series resistor representing the
 123 cell ohmic resistance. This resistance is a function of the cell temperature. The third term is
 124 the polarization overvoltage, accounting for charge transfer, electrochemical double layer and
 125 diffusion phenomenon. It is represented in the equivalent circuit by a series of R-C parallel
 126 circuits of voltage η_j and time constants $\tau_j = R_j C_j$. They account for transient dynamics and the
 127 voltage drop over each circuit is described by Eq. 4. In this study, three R-C parallel circuits are
 128 used for a good trade-off between low computation time and high precision as recommended in
 129 [36]. The value of time constants τ_j are fixed and the resistances R_j are considered as a function
 130 of cell temperature, SOC, current rate and direction of the current (charge or discharge).

$$SOC = SOC_{ini} + \frac{1}{3600Q_c} \int Idt. \quad (2)$$

$$\eta_{\Omega} = R_{\Omega}I. \quad (3)$$

$$\tau_j \frac{d\eta_j}{dt} = -\eta_j + R_j I. \quad (4)$$

131 The thermal model is a one-state lumped-parameters model. It computes the evolution of the
 132 cell temperature T_c (in kelvins) depending on the ambient temperature T_{ext} and generated heat
 133 \dot{Q}_{gen} (in watts) as described by

$$m C_p \frac{dT_c}{dt} = \dot{Q}_{gen} + h S (T_{ext} - T_c), \quad (5)$$

134 where C_p (in $\text{J K}^{-1} \text{kg}^{-1}$) is the cell specific heat capacity, m (in kg) is the cell mass, S (in
 135 m^2) is the cell external surface and h (in $\text{W K}^{-1} \text{m}^{-2}$) is the heat transfer coefficient between the
 136 cell and its outside environment, which accounts for thermal exchanges by convection, radiation
 137 and conduction. The generated heat \dot{Q}_{gen} is described by Eq. 6. The first term corresponds to
 138 joule heat and comes directly from the electrical model. The second term corresponds to entropy
 139 heat, where the coefficient $\frac{\partial U_{oc}}{\partial T}$ is a function of SOC.

$$\dot{Q}_{gen} = I(U - U_{oc}) + I T_c \frac{\partial U_{oc}}{\partial T}. \quad (6)$$

140 A high energy 3 Ah 18650 cell is considered throughout this article. The cell is further
 141 presented in the experimental section (refer to 3.1). Several methods from the literature were
 142 used to identify the model parameters. The open-circuit voltage U_{oc} and cell capacity Q_c were
 143 identified during an incremental charge with relaxation periods [37]. The resistances R_Ω , R_j
 144 and time constants τ_j were identified during electrochemical impedance spectroscopy tests as
 145 well as charge/discharge pulses and relaxations tests [33]. These tests were realized at several
 146 temperatures (between -15°C and 45°C), several SOC (between 0 % and 100 %) and several
 147 current values (between 1.5 A and 7.5 A), to obtain a lookup table of impedance parameters
 148 values at different operating conditions. Specific heat capacity C_p and heat transfer coefficient h
 149 were obtained during a heating test by application of a squared alternative current [38]. Finally,
 150 the entropy heat coefficient $\frac{\partial U_{oc}}{\partial T}$ was identified during potentiometric measurements of open-
 151 circuit voltage at different temperatures and SOC [39]. Calibration procedure of the electro-
 152 thermal model and identified parameters are further described in supplementary materials (refer
 153 to Appendix).

154 Based on the described models, a simulator is coded into the SIMULINK environment. The
 155 functional coupling between electrical and thermal models is illustrated by Figure 2 and works as

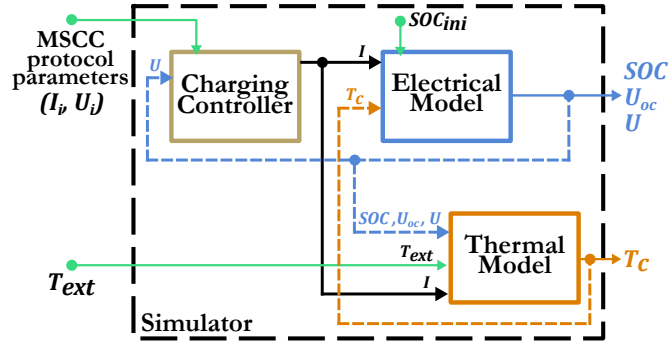


Figure 2: Schematic representation of the simulator developed to emulate battery behavior during MSCC charge.

156 described in the following. Depending on the applied current, the electrical model first computes
 157 SOC and U based on values of U_{oc} , R_{Ω} and R_i at this SOC and T_c . The values of SOC , U_{oc} and
 158 U are then passed onto the thermal model, which computes \dot{Q}_{gen} and then T_c . The value of T_c
 159 finally comes back into the electrical model to compute the new values of resistances parameters.
 160 Upstream from the coupled electro-thermal model, a charge controller block is integrated to
 161 determine the applied current based on a CC-CV or MSCC protocol.

162 To verify the model validity for the study of fast charging, experimental CC-CV charges at
 163 three current values (1.5, 3.0 and 6.0 A, corresponding to C/2, 1C and 2C) and at three ambient
 164 temperatures (0, 20 and 40 °C) were realized and compared to simulation results. Comparison
 165 results are given as supplementary files to this article (refer to Appendix). Results show that the
 166 model accurately predicts the cell voltage (with an error range of 24-46 mV), as well as the cell
 167 temperature (with an error range of 0.2-1.2 °C) and charging time for the 9 tests. Hence, the
 168 coupled electro-thermal model is suited to our investigation of fast charging at different temper-
 169 atures.

170 2.3. Constrained optimization problem

171 This subsection formulates a constrained optimization problem [40] to define the parameters
 172 of a MSCC charging protocol, using the battery model described above. No aging model is used
 173 in this article; instead, battery aging is taken into account in an implicit manner, in the different
 174 costs and constraints. Proceeding this way allows to promptly reuse its results for another cell
 175 reference, without needing to calibrate a new aging model.

176 2.3.1. *Costs*

177 Costs are mathematical functions to be minimized. In the literature on optimized charging
 178 protocol cited in the introduction, several costs are frequently considered. All references used
 179 a cost on charging time [14, 16, 17, 25–28], two used a cost on energy losses during charging
 180 [25, 27], three used a cost on cell temperature rise [14, 25, 26], and three used a cost on cell
 181 degradation when using an aging model [17, 27, 28]. In the present paper, charging time is
 182 rather chosen as a constraint and two distinct costs are considered. These two cost functions are
 183 dependent on the vector of optimization variables \vec{x} , which are the currents of each step of the
 184 MSCC protocol.

185 The first cost is a cost on energy losses J_{el} due to joule effect, which exists in the literature.
 186 This cost is computed by integration of overvoltages during the whole charge duration as ex-
 187 pressed by Eq. 7. The effect of J_{el} is to reduce the charging current and it is more important
 188 when the internal resistance is higher, such as at low SOC and low temperatures [33].

$$J_{el}(\vec{x}) = \int_{t_0}^{t_f} (U(t) - U_{oc}(t)) I(t) dt. \quad (7)$$

189 The second cost is a cost on end-of-charge overvoltages J_{eoc} . Relative to existing literature, it
 190 is a novel proposition to limit aging mechanisms accelerated by fast charging at high SOC such as
 191 lithium plating or SEI growth. To determine what SOC range corresponds to the final part of the
 192 charge for a given cell, we propose to use differential voltage analysis [41] from a low current
 193 charge as plotted on Figure 3 for the studied cell. Several distinctive features of the positive
 194 and negative electrodes can be observed on Figure 3b. More specifically, the position of the
 195 central graphite peak is highlighted. This peak corresponds to a half-lithiated graphite (LiC_{12}),
 196 and signals the start of the potential plateau corresponding to the transition of graphite from this
 197 stage to the fully lithiated stage (LiC_6) [42]. As this plateau is the closest to the potential of
 198 lithium plating, the position of the central graphite peak can be used as a signal for the beginning
 199 of the last part of charging. This peak is positioned at 50 % of graphite SOC, but can change
 200 for the full cell depending on the balancing between positive and negative electrodes. For the
 201 studied cell, it is located at 57 % (Figure 3b). The cost J_{eoc} is finally computed with Eq. 8, by
 202 an integration in the SOC domain of overvoltages multiplied by a penalty function P_{eoc} . This
 203 penalty function is calculated by Eq. 9, where γ_{SOC} is the SOC of the central graphite peak
 204 as highlighted on Figure 3b. Thus, the effect of J_{eoc} is to reduce the charge current after the

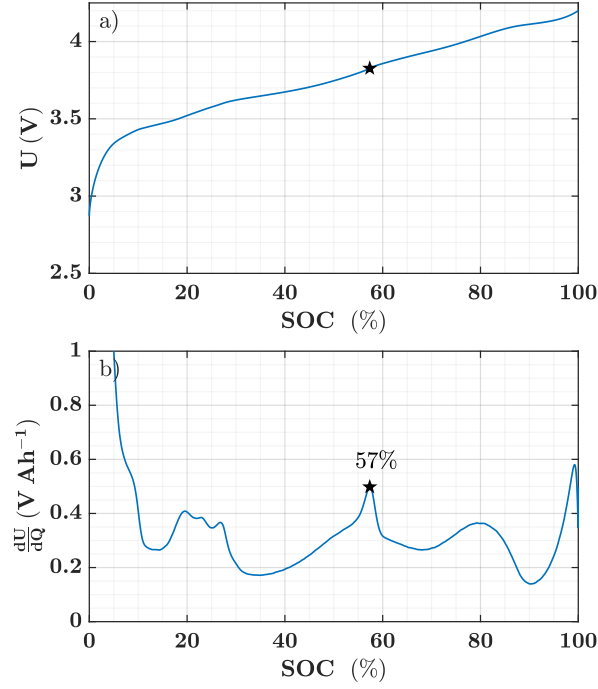


Figure 3: Position of the LiC_{12} graphite peak on the SOC scale: (a) cell voltage during a C/10 charge at 25 °C and (b) corresponding differential voltage with position of central graphite peak highlighted.

205 beginning of last graphite transition and it increases towards higher SOC.

$$J_{eoc}(\vec{x}) = \int_{SOC_0}^{SOC_f} (U(SOC) - U_{oc}(SOC)) P_{eoc}(SOC) dSOC. \quad (8)$$

$$P_{eoc}(SOC) = \begin{cases} 0, & \text{if } SOC < \gamma_{SOC}, \\ (SOC - \gamma_{SOC})^3, & \text{if } SOC \geq \gamma_{SOC}. \end{cases} \quad (9)$$

206 As expressed by equations 7 and 8, the two cost functions J_{el} and J_{eoc} can have very different
 207 numerical values, which can be delicate to balance. To avoid this issue, we propose to normalize
 208 them by introducing limits on the optimal charge to be found. An inferior limit would be a
 209 normal charge, with a charging time just below of what could be considered as fast charging. For
 210 a high energy cell as the one studied, we choose a CC-CV protocol with a current rate of C/2
 211 (meaning here a current of 1.5 A) for a slowest charge possible of around 2 hours. A superior

212 limit would be the fastest charge possible. Of all conceivable definitions, the highest current
 213 profile possible without exceeding the upper voltage limit of the cell (here 4.2 V) is chosen. This
 214 can be obtained by achieving a CV charge directly from the discharged state. These two charges
 215 can be simulated with the model and Figure 4 represents their obtained current profiles in the
 216 time and SOC domains. The defined upper limit charge leads to extremely high currents which
 217 would not be safe for the cell. This charge should thus be considered as a theoretical high limit
 218 for current and low limit for charging time (here 29 min at 25 °C). These two charge limits can
 219 be simulated for each simulation condition to obtain the value of $J_{i,lb}$ and $J_{i,ub}$, where J_i is either
 220 J_{el} or J_{eoc} . These values finally allow to normalize the cost function with Eq. 10. The normalized
 221 costs \tilde{J}_i thus vary between 0 and 1. Consequently, the optimal fast-charge protocol should have
 222 a current profile that is between the two curves on Figure 4b, for a charge duration between the
 223 two bounds on Figure 4a.

$$\tilde{J}_i = \frac{J_i - J_{i,lb}}{J_{i,ub} - J_{i,lb}}. \quad (10)$$

224 The next step is to construct the objective function f that is to be minimized by weighting
 225 the individual costs as expressed by

$$f(\vec{x}) = \omega_{el}\tilde{J}_{el} + \omega_{eoc}\tilde{J}_{eoc}, \quad (11)$$

226 where ω_{el} and ω_{eoc} are the weights respective to costs \tilde{J}_{el} and \tilde{J}_{eoc} . The vector of weights is
 227 noted $\vec{\omega} = [\omega_{el}, \omega_{eoc}]$. Figure 5 reports the evolution of the individual cost functions versus the
 228 CC current of CC-CV charge protocol in the range 1.5 A (C/2) to 9 A (3C). It can be observed
 229 that the cost \tilde{J}_{eoc} is higher and increases faster with charge current compared to the cost \tilde{J}_{el} . Thus,
 230 it is possible to use a higher weight on \tilde{J}_{el} to balance the two objectives.

231 Due to their numerical nature, the allocation of weights requires prior numerical experiments
 232 and should depend on the relative importance of cost \tilde{J}_{el} and \tilde{J}_{eoc} to the user of the method. As
 233 we stated for the costs in Section 2.3.1, allocating a higher weight ω_{el} will tend to reduce the
 234 current more towards low SOCs, whereas allocating a higher weight ω_{eoc} will tend to reduce the
 235 current more towards high SOCs. Ultimately, we chose to allocate a higher weight on \tilde{J}_{el} to put
 236 an emphasis on relatively higher currents towards higher SOCs because for real electric vehicle,
 237 charging will rarely start from very low SOCs, which limits the benefits of charging protocols
 238 that make use of very high current values at low SOCs to reduce total charging time (such as

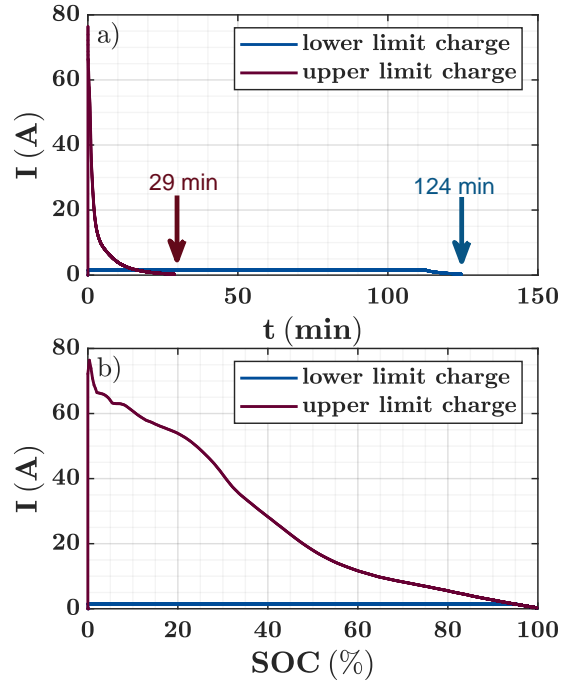


Figure 4: Limits on optimal charge search: simulated current profiles of lower limit charge and upper limit charge as a function of (a) time and (b) SOC (example at 25 °C). The reader is advised that the upper limit charge leads to an extremely high current peak at the beginning of charge and should be considered as a theoretical case (here simulated), as charging a cell at such rates could lead to safety issues.

239 those resulting from a higher weight on \tilde{J}_{eoc} here). All in all, the weights $\vec{\omega} = [0.8, 0.2]$ are used
 240 in the rest of this article.

241 2.3.2. Constraints

242 With the objective function defined, we propose a constrained optimization problem to de-
 243 termine the parameters of a MSCC fast charging protocol. The considered problem is expressed
 244 as follows

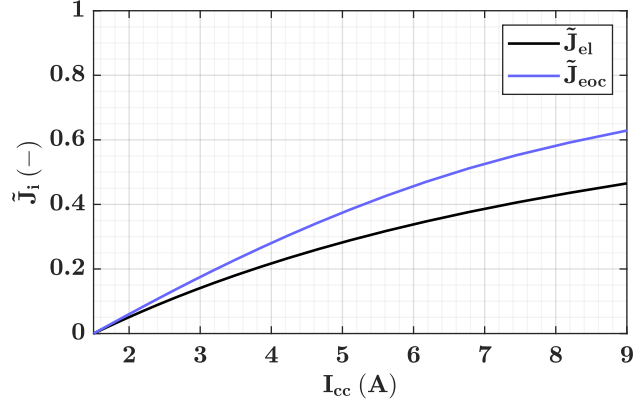


Figure 5: Evolution of individual normalized cost functions \tilde{J}_{el} and \tilde{J}_{eoc} as a function of CC current I_{cc} of CC-CV charge protocol.

$$\min_{\vec{x}=[I_1, I_2, \dots, I_3]} f(\vec{x}) \quad (12a)$$

$$\text{subject to: } t_f \leq t_{max}, \quad (12b)$$

$$SOC_f \geq SOC_{min}, \quad (12c)$$

$$T_c(t) \leq T_{max} \quad \forall t \in [t_0; t_f], \quad (12d)$$

$$\Delta T_c(t) \leq \Delta T_{max} \quad \forall t \in [t_0; t_f], \quad (12e)$$

$$I_{lb} \leq I_i \leq I_{ub} \quad \forall i \in \llbracket 1; n \rrbracket, \quad (12f)$$

$$I_m > I_{m+1} > \dots > I_n \quad \text{with } m \in \llbracket 1; n \rrbracket. \quad (12g)$$

245 Differently from previous references in the literature, charge duration is here taken solely
 246 as a constraint. Eq. 12b means that a maximal charging time t_{max} is set, which leads to higher
 247 currents and counterbalances the objective function f . This constraint should be chosen between
 248 the two bounds of Figure 4a (29 min and 124 min) for an achievable target in charging time.

249 The second constraint in Eq. 12c is on a minimal SOC at end-of-charge SOC_{min} . This
 250 constraint compensates the charging time constraint and ensures that a minimum of capacity or
 251 energy is charged.

252 The third and fourth constraints are thermal constraints. Eq. 12d sets a maximal cell tem-
 253 perature T_{max} to not exceed. Eq. 12e sets a maximal heating ΔT_{max} , to also limit self-heating at

254 colder temperatures.

255 The fifth constraint sets bounds on current value in Eq. 12f. A lower bound I_{lb} helps to avoid
256 very low currents that prolongs charging time. An upper bound I_{ub} allows to avoid excessive
257 currents.

258 Finally, a sixth constraint is used in Eq. 12g on the regularity of current decrease in the
259 successive steps of the MSCC protocol. The step m where the regularity constraint starts to take
260 effect can be chosen. For example, setting $m = 1$ forces a regular decline from a first step to
261 obtain a current profile similar as [21]. Otherwise, it is possible to set $m > 1$ to let the liberty for
262 an inferior current at beginning-of-charge to obtain a current profile similar to [16].

263 2.3.3. Optimization algorithm

264 The optimization is based on the cell model described in 2.2 by linking the SIMULINK model
265 to the MATLAB environment. The optimization algorithm used is the `fmincon` function with the
266 interior points method. The gradients of the objective function and non-linear constraints (Eq.
267 12b, 12c, 12d and 12e) are computed numerically with the central finite differentiation method
268 and are fed to `fmincon` at each iteration. From a given initial value of MSCC currents \vec{x}_0 , the
269 optimization algorithm thus runs charge simulations to obtain information on objective function,
270 constraints and their gradients, and then decides a new iterates until stopping criteria are met and
271 an optimal solution \vec{x}_* is found.

272 2.4. Example of numerical results

273 To better understand the operation of the optimization algorithm according to the set of equa-
274 tions 12, a case study is proposed with a MSCC protocol of two stages. The two-dimensional
275 case gives an intuition about the influence of constraints on the solution. Two constraints are con-
276 sidered here, one on the charge duration $t_f \leq 45$ min, and the other on the final state-of-charge
277 $SOC_f \geq 90$ %.

278 Figure 6a draws the contours of the objective function f and the position of the two con-
279 straints. The objective function tends to decrease when both currents I_1 and I_2 decrease. The
280 constraint on the final state-of-charge SOC_f only depends on the current of the last stage I_2 .
281 All values of I_2 that are above this constraint do not respect the condition $SOC_f \geq 90$ %. On
282 the other hand, the constraint on the charge duration t_f depends on the value of the current in
283 all stages. All combinations of I_1 and I_2 that are located left and below this constraint do not

284 respect the condition $t_f \leq 45$ min. The feasible solutions are thus combinations of I_1 and I_2 that
 285 are located between the two constraints lines in the low-right corner. As f decreases with lower
 286 values of I_1 and I_2 , the optimal solution to problem 12 is located at the intersection of the two
 287 constraints.

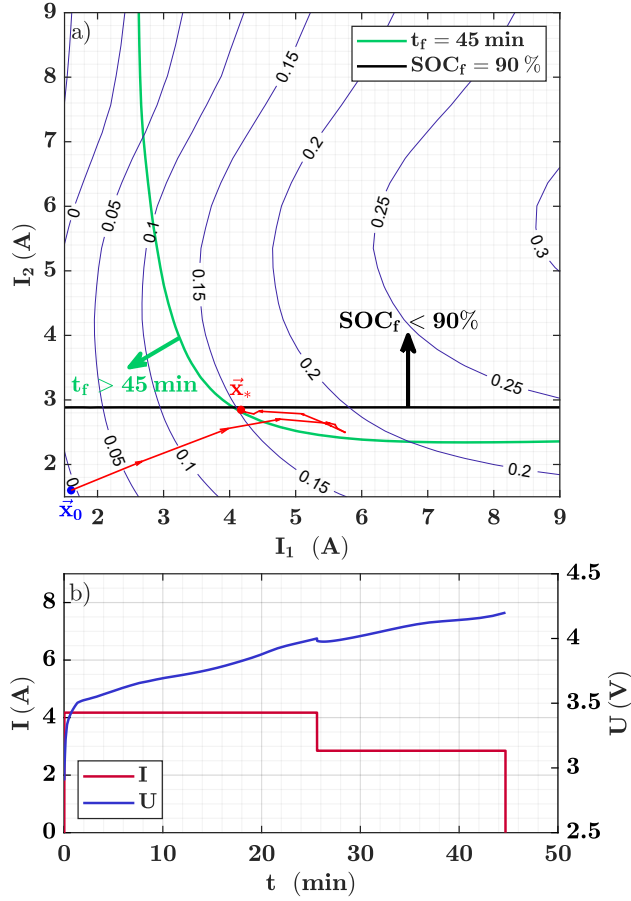


Figure 6: Example of numerical results for MSCC protocol with 2 steps ($n = 2$, $U_1 = 4.0$ V, $U_2 = 4.2$ V, $\vec{\omega} = [0.8, 0.2]$, $T_{ext} = 25$ °C): (a) contours of the objective function f , constraints on charge duration t_f , and final state-of-charge SOC_f and iterations from initial vector \vec{x}_0 to optimal solution \vec{x}_* , (b) current and voltage profiles of optimal protocol.

288 Figure 6 also depicts the iterations of the optimization algorithm from an initial guess \vec{x}_0 to
 289 the found solution \vec{x}_* . It can be seen that the algorithm first seeks to respects all constraints and
 290 then seeks to minimize f inside the feasible domain. The final iterate \vec{x}_* is indeed found at the

291 intersection of the two constraints. Figure 6b finally reports the simulated current and voltage
292 profiles of the corresponding optimal protocol.

293 The same principle holds for a higher number of stages in the MSCC protocol. In the follow-
294 ing, this method is exploited to define several fast charging MSCC protocols with 5 or 10 stages
295 as case studies to experimentally investigate the impact of protocols defined by this method on
296 aging.

297 **3. Experimental aging tests**

298 This section describes the experimental tests conducted to verify the impact of optimized
299 MSCC fast charging protocols on battery lifetime. They are compared with fast charging CC-
300 CV protocols, considered as baseline conditions.

301 *3.1. Studied cell*

302 The cell reference INR18650HG2 from LG is selected to conduct aging experiments. Table 1
303 details its specifications. It is a 3 Ah cell in the 18650 cylindrical format, with a nickel-rich
304 $\text{LiNi}_{0.8}\text{Mn}_{0.1}\text{Co}_{0.1}\text{O}_2$ (NMC) positive electrode and a blended graphite-silicon oxide (G-SiO)
305 negative electrode. Its materials and high energy density make it suited to battery electric vehicles
306 with high driving autonomy.

307 The manufacturer recommends both a standard charge current and a fast-charge current of
308 respectively 1.5 A (C/2) and 4 A (1.33C). Hence, we expect 4 A to be representative of fast
309 charging for this cell.

310 *3.2. Optimized MSCC and reference CC-CV charging protocols*

311 Five fast charging MSCC protocols are defined by using the numerical optimization problem
312 presented in Section 2 and compared to four reference CC-CV protocols under similar operating
313 conditions.

314 *3.2.1. Common parameters for optimized MSCC protocols*

315 For the definition of optimized MSCC protocols, several parameters are kept constant be-
316 tween all conditions: the voltage thresholds and several constraints.

317 The number of stages is set to $n = 10$ for cases of complete charge. This number of stages
 318 allows sufficient tuning of the current on different SOC ranges while not significantly increas-
 319 ing the convergence time of the optimization algorithm for too small current variations between
 320 stages. With the number of stages set to ten, several options can be considered for setting voltage
 321 thresholds values U_i such as increments of voltage, or increments of SOC or energy and corre-
 322 sponding changes in the cell OCV. The issue with using, for example, fixed voltage increments
 323 between stages is that the first stages are completed very rapidly due to high overvoltages and
 324 represent a small portion of the charged capacity, while last stages either significantly extend the
 325 charging duration or cut the charge short. Thus, more discretization is needed for the high volt-
 326 age range. Ultimately, we opted for progressively decreasing voltage increments between each
 327 stage which resulted in the voltage thresholds detailed by Table 2. They allow for a high amount
 328 of capacity to be charged in the first stages and for adaptation of the current in the last stages in
 329 the high voltage range. Moreover, as the cell upper voltage limit U_{max} is progressively reached,
 330 no prolonged charging happens at U_{max} such as in a CC-CV protocol. Thus, these thresholds can
 331 help to limit aging due to high overvoltages towards end-of-charge. All in all, this choice helps
 332 to better balance the three main objectives of low charging time, high capacity charged, and low
 333 degradation. The voltage thresholds in Table 2 are related to the specific OCV features of the
 334 studied NMC/G-SiO cell, which is relatively linear in its 10%-100% SOC range [43], and should
 335 be adapted depending on the electrodes' materials.

336 To limit aging as well, four constraints are set. Thermal constraints of Eq. 13 and 14 require

Table 1: Specifications of the cell investigated in aging tests.

Reference	LG INR18650HG2
Positive material	LiNi _{0.8} Mn _{0.1} Co _{0.1} O ₂ (NMC)
Negative material	Graphite + SiO (G-SiO)
Nominal capacity	3000 mAh
Energy density	240 Wh kg ⁻¹
Voltage range [U_{min}, U_{max}]	2.5 to 4.2 V
Charge temperature range	0 to 50 °C
Standard charge current	1.5 A (C/2)
Fast charge current I_{fc}	4 A (1.33C)

337 the cell temperature to be inferior to 50 °C and to not rise more than 15 °C relative to the ambient
338 temperature. The current levels of each stage are bounded between 300 mA (C/10) and 9 A (3C)
339 as set by Eq. 15. Finally, constraint of Eq. 16 forces the current to decrease regularly starting
340 from the second stage, while current I_1 is let free.

$$T_c(t) \leq 50^\circ\text{C} \quad \forall t \in [0; t]. \quad (13)$$

$$\Delta T_c(t) \leq 15^\circ\text{C} \quad \forall t \in [0; t]. \quad (14)$$

$$C/10 \leq I_i \leq 3C \quad \forall i \in \llbracket 1; n \rrbracket. \quad (15)$$

$$I_2 > I_3 > \dots > I_n. \quad (16)$$

341 3.2.2. Experimental conditions for reference and optimized charging protocols

342 Four CC-CV protocols are selected to offer comparison with MSCC optimized protocols.
343 They were previously investigated in one of our aging studies among other protocols [31]. Their
344 experimental conditions, charge durations and final SOCs are given in Table 3. Three parameters

Table 2: Voltage thresholds of stages of optimized MSCC protocols.

U_{stage}	Voltage (V)
U_1	3.60
U_2	3.90
U_3	4.00
U_4	4.05
U_5	4.10
U_6	4.12
U_7	4.14
U_8	4.16
U_9	4.18
U_{10}	4.20

Table 3: Experimental conditions for reference CC-CV protocols and experimentally measured charge duration t_f and final state-of-charge SOC_f .

Condition	T_{ext} (°C)	I_{cc} (A)	U_{cv} (V)	t_f (min)	SOC_f (%)
1	25	4 (1.33C)	4.2	61	96.2
2	25	5 (1.66C)	4.1	46	83.3
3	5	4 (1.33C)	4.2	66	91.4
4	45	4 (1.33C)	4.2	53	97.8

are varied: the ambient temperature T_{ext} , the CC stage current I_{cc} , and the CV stage voltage U_{cv} . The chosen temperatures of 5, 25, and 45 °C represent a cold, mild, and hot climate, respectively. Because of reduced internal resistance when ambient temperature increases, the charge duration decreases and the final state-of-charge increases. Most conditions are achieved at the recommended fast charging current of $I_{cc} = 4$ A (1.33C) during CC stage and at the maximum cell voltage of $U_{cv} = 4.2$ V during CV stage, with charging stopped when the current is lower than $I_{cv} = 300$ mA (C/10), in order to represent near complete charge at the selected temperatures. Parameters I_{cc} and U_{cv} are changed for condition 2, to have one partial charge condition at 25 °C.

Five simulation conditions are given to the optimization algorithm to obtain five optimized MSCC protocols. Three key parameters are modified: the ambient temperature T_{ext} , the constraint on charge duration t_f , and the constraint on final state-of-charge SOC_f . These conditions are summarized in Table 4 as well as the t_f and SOC_f of the defined protocols measured in experimental conditions. The simulated current profiles of defined optimized protocols are pictured in Figure 7b. These conditions are chosen to allow for an objective comparison with fast charging CC-CV protocols (Table 3) in terms of thermal conditions, charge duration and capacity charged, with the objective to either decrease the charge time and/or the degradation compared to CC-CV protocols. Each comparison is explained in the following paragraphs.

3.2.3. Description of the compared charging protocols

Condition CC-CV 1 is considered to investigate the impact of a near complete charge at 25 °C. It is compared to conditions MSCC A and MSCC B, which aim to decrease the degradation in a similar charge duration of around 60 min or to reduce the charge duration to around 50 min,

Table 4: Experimental conditions for optimized MSCC protocols and experimentally measured charge duration t_f and final state-of-charge SOC_f .

Condition	T_{ext} (°C)	$t_f \leq$ (min)	$SOC_f \geq$ (%)	n (-)	t_f (min)	SOC_f (%)
MSCC A	25	60	98	10	65	96.8
MSCC B	25	50	98	10	52	93.5
MSCC C	25	35	80	5	37	78.4
MSCC D	5	90	95	10	91	90.4
MSCC E	45	45	98	10	44	95.1

367 respectively. As an example, simulated current and voltage profiles of MSCC A are shown in
368 Figure 7a.

369 Condition CC-CV 2 is considered to treat a case of partial charge at 25 °C. A higher current
370 of $I_{cc} = 5$ A (1.66C) is used in the CC stage and a reduced voltage $U_{cv} = 4.1$ V is used in the
371 CV stage. These parameters lead to a 15 min faster charge than the complete charge at the same
372 ambient temperature but with slightly less capacity charged. It is compared to condition MSCC
373 C, which aims to further decrease the charge duration by 10 min. The number of stages is limited
374 to $n = 5$ in this case, to operate on the same voltage window as its CC-CV reference.

375 Condition CC-CV 3 is considered to investigate the impact of a near complete charge at a
376 cold temperature of 5 °C. It is compared to condition MSCC D, which aims to decrease the
377 degradation. As previous tests with the CC-CV protocol (charging in 66 min) showed that the
378 cell aged very rapidly [31], the charge duration constraint was relaxed to 90 min.

379 Condition CC-CV 4 is considered to investigate the impact of a near complete charge at a hot
380 temperature of 45 °C. It is compared to conditions MSCC E, which aims to decrease the charge
381 duration to around 45 min. Thanks to improved kinetics at elevated temperature, this charge
382 duration (while respecting SOC_f constraint) can be reached without touching the upper bound
383 on current, contrarily to condition MSCC B and C at 25 °C (see Figure 7b).

384 Five optimized fast charging MSCC protocols are obtained in this manner. Their current
385 profiles are vastly different compared to reference CC-CV protocols (Figure 7b). Also, several
386 MSCC protocols significantly exceed the maximum current value of 4 A recommended by the
387 cell manufacturer (Table 1). A cycling aging campaign was performed to verify the impact of

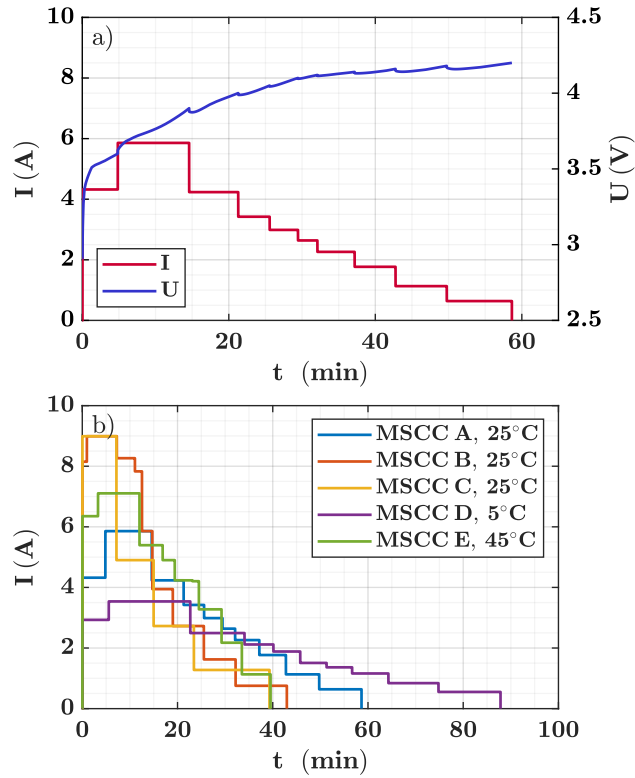


Figure 7: Optimized MSCC protocols for aging experiments: (a) simulated current and voltage profiles of MSCC A and (b) simulated current profiles of all conditions as a function of charge time.

388 such protocols on aging.

389 3.3. Aging tests procedure

390 Experimental cycle aging tests are performed by repeating a charge-pause-discharge-pause
 391 sequence. The charge step is either one of the reference CC-CV protocols (conditions 1, 2, 3, 4)
 392 or one of the optimized MSCC protocols (conditions A, B, C, D, E). In total, 9 tests are carried
 393 out. Discharges are identical for all tests and are done in a CC protocol with a current of 1.5 A
 394 ($C/2$). Charges and discharges are separated by 15 min pauses to allow the cells to cool down to
 395 ambient temperature.

396 Each test is performed on two different new cells to verify repeatability. All cells were
 397 pre-screened. The preliminary inspections showed that cell-to-cell variations in capacity and

398 resistance were low and could be neglected compared to the difference in cycle life caused by
399 different charging protocols. Thus, clear conclusions could be drawn from the comparison of
400 aging caused by optimized MSCC protocols and reference CC-CV protocols.

401 While considering test equipment, cycling is conducted with Biologic BCS-815 power benches
402 connected electrically to the cells with Biologic BH-1i holders. Cells are placed inside Climats
403 thermal chambers to regulate temperature at the ambient temperature T_{ext} .

404 3.4. Characterization procedure

405 Initial, periodic and final characterizations are performed at a temperature of 25 °C. Cycling
406 tests are interrupted around every 10 days for the characterizations. Their goal is to provide a
407 reference measure of capacity and its evolution with aging under comparable conditions. Capac-
408 ity Q_{dch} is measured during a CC discharge at C/10 until U_{min} , after the cells have been charged
409 by a CC charge at C/10 until U_{max} . The relative capacity based on this measure is used in the
410 following section to assess aging caused by fast charging protocols.

411 4. Experimental aging results and discussions

412 This section reports the experimental results and further discusses them. Results of opti-
413 mized MSCC protocols and reference CC-CV protocols are compared on Figure 8. The two left
414 columns of Figure 8 compare the charge current profiles, as a function of time and of SOC, for
415 one charge event. The right column reports the evolution of relative capacity as a function of the
416 number of accumulated charge/discharge cycles.

417 4.1. Case A (25 °C)

418 The protocol MSCC A is compared with the CC-CV protocol of parameters $T_{ext} = 25$ °C,
419 $I_{cc} = 4$ A, $U_{cv} = 4.2$ V, and $I_{cv} = 0.3$ A. The current profiles are compared on Figure 8a and
420 Figure 8b. Charging time of protocol MSCC A is 65 min, which is 4 min longer than its reference
421 CC-CV protocol. The current of the MSCC protocol becomes inferior to that of CC-CV after a
422 SOC of 58 %. This result can be attributed to the cost on end-of-charge overvoltage introduced
423 in 2.3.1.

424 Evolutions of relative capacity are compared on Figure 8c. From the beginning of cycling,
425 protocol MSCC A degrades the cell less than the CC-CV protocol, with 3 % less capacity loss.

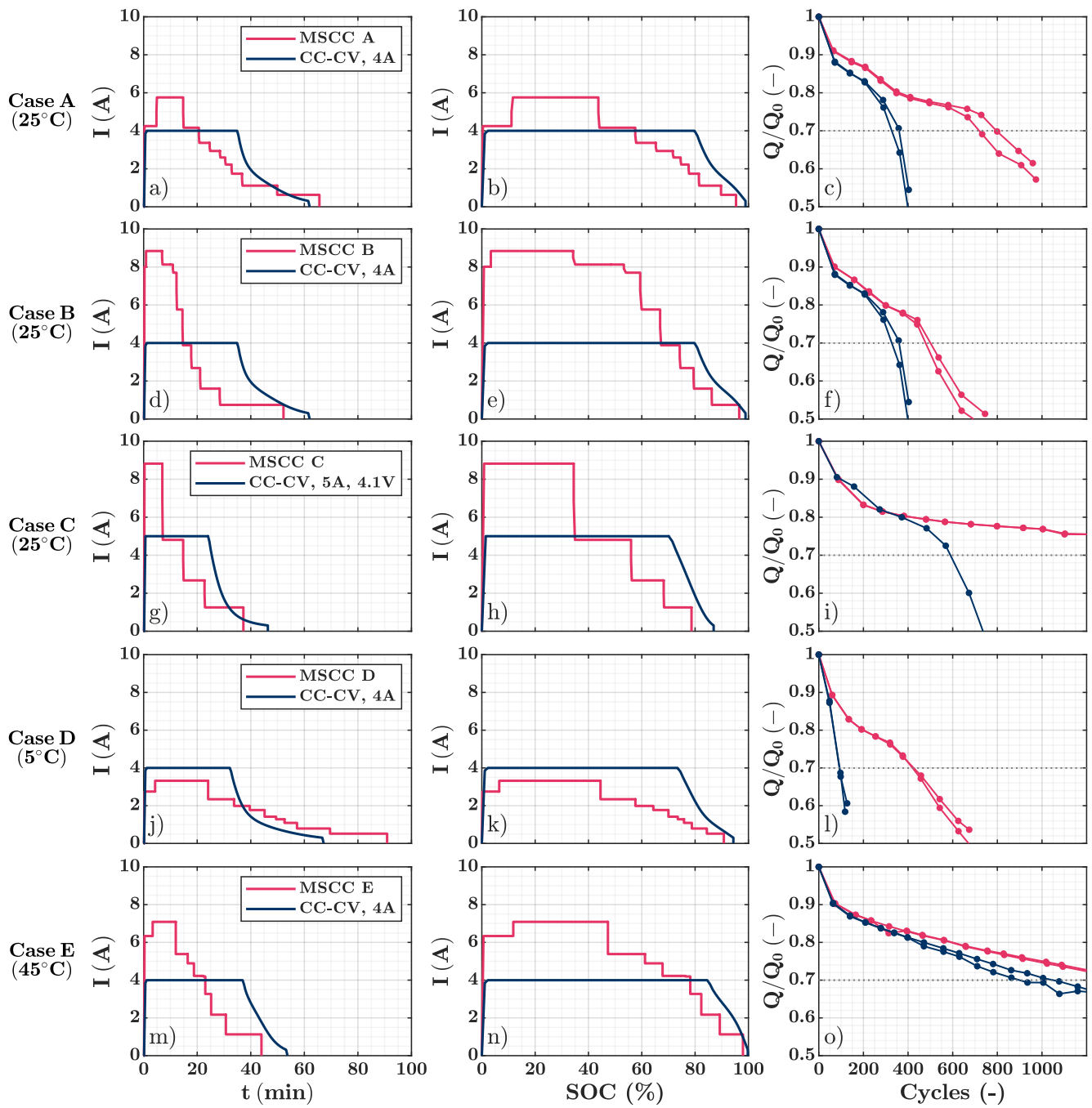


Figure 8: Comparison of experimental charging and aging results between CC-CV reference protocols and optimized MSCC protocols: (left) charge current as a function of time, (center) charge current as a function of SOC and (right) evolution of relative capacity as a function of cycle number. Each row compares one case of MSCC protocol with a corresponding CC-CV protocol.

426 The degradation stays inferior to that of CC-CV after that, and the MSCC A protocol even
427 postpones and limits the sharp acceleration of capacity loss caused by CC-CV protocol below a
428 remaining capacity of 80 %. This capacity rollover, that can be observed for both protocols, is
429 indicative of lithium plating [44, 45]. Thus, although MSCC A protocols did not avoid lithium
430 plating, it allowed to reduce its amount while charging in a similar duration. This result can
431 be attributed to the significant reduction of MSCC current after 58 % of SOC. Considering an
432 end-of-life criterion of 70 % remaining capacity (30 % capacity loss), cells cycled under CC-CV
433 protocol reached end-of-life after around 330 cycles and those cycling with MSCC A between
434 700 and 800 cycles.

435 4.2. Case B (25 °C)

436 The protocol MSCC B is compared to the same CC-CV protocol and their current profiles
437 are compared on Figure 8d and Figure 8e. Charge duration of protocol MSCC B is of 52 min,
438 inferior by 9 min to that of its reference CC-CV protocol. To achieve this low charging time, the
439 current values of MSCC A are more than two times superior to that of CC-CV (superior to 8 A)
440 during a significant part of the charge, which corresponds to 53 % of the capacity. The current
441 also becomes inferior to that of the CC-CV protocol after 74 % of SOC, thus 16 % later than
442 MSCC A.

443 Evolutions of relative capacity are compared on Figure 8f. When compared with MSCC A
444 (Figure 8c), it can be seen that the lower charge duration of MSCC B negatively impacts the
445 cycle life. Nevertheless, it can also be observed that the significantly lower charging time and
446 higher currents for 74 % of charged capacity did not increase the degradation when compared to
447 the reference CC-CV protocol. After a relatively similar capacity loss at beginning of cycling,
448 the MSCC B gradually degrades less than the CC-CV reference. Cells cycled under MSCC B
449 protocol reached end-of-life after around 450 cycles.

450 4.3. Case C (25 °C)

451 The protocol MSCC C is compared to the CC-CV protocol of parameters $T_{ext} = 25$ °C,
452 $I_{cc} = 5$ A, $U_{cv} = 4.1$ V and $I_{cv} = 0.3$ A. The charge is stopped at a partial SOC for the two
453 protocols. Their current profiles are compared on Figure 8g and Figure 8h. The charging time
454 of MSCC C protocol is only 37 min, 9 min lower to that of the CC-CV reference. Current of
455 MSCC C becomes inferior to that of CC-CV after 56 % SOC. The final SOC of protocol MSCC

456 C is lower by 5 % compared to that of the CC-CV reference, which can be quite significant
457 considering the impact of depth-of-cycling on aging [46].

458 Evolutions of relative capacity are compared on Figure 8i. The degradation caused by the
459 two protocols is similar at the beginning of cycling. At 80 % remaining capacity and below,
460 however, the degradation caused by MSCC C considerably slows while that caused by the CC-
461 CV reference sharply increase. This result can potentially be explained by the lower final SOC
462 of MSCC protocol, which cause the cell to charge less on SOC interval where aging mechanisms
463 such as lithium plating can occur. Cells cycled under the CC-CV protocol reached end-of-life
464 after around 600 cycles, whereas cells cycled under MSCC C protocol only lost 25 % of their
465 capacity after 1200 cycles.

466 4.4. Case D (5 °C)

467 For cases at low temperature, the protocol MSCC D is compared to the CC-CV protocol of
468 parameters $T_{ext} = 5\text{ °C}$, $I_{cc} = 4\text{ A}$, $U_{cv} = 4.2\text{ V}$, and $I_{cv} = 0.3\text{ A}$. Their current profiles are
469 compared on Figure 8j and Figure 8k. The charge duration of MSCC D is 91 min, which is 25
470 min slower than its CC-CV reference. Therefore, the current of MSCC D is always inferior to
471 the CC-CV protocol in the SOC domain.

472 Evolutions of relative capacity are compared on Figure 8l. The CC-CV protocols caused
473 massive degradation to the cells, characterized by a sharp drop of capacity. This shows that
474 the studied cell is highly impacted by fast charging at low temperatures. The MSCC D protocol
475 reduced aging significantly. The first part of degradation, characterized by a decrease of the speed
476 of capacity loss, can be observed, similar to results at higher temperatures. Then, at around 75
477 % remaining capacity, the capacity loss accelerates strongly again. All in all, the end-of-life
478 is reached after around 100 cycles for the CC-CV reference and after around 400 cycles for
479 the MSCC D protocol. Thus, an adapted charge duration and lower current rates allowed to
480 significantly improve the cells lifetime.

481 4.5. Case E (45 °C)

482 For cases at high temperature, the protocol MSCC E is compared to the CC-CV protocol
483 of parameters $T_{ext} = 45\text{ °C}$, $I_{cc} = 4\text{ A}$, $U_{cv} = 4.2\text{ V}$, and $I_{cv} = 0.3\text{ A}$. Their current profiles
484 are compared on Figure 8m and Figure 8n. The MSCC E protocol completes the charge in 44

485 min, which is 9 min lower compared to the CC-CV reference. The current of MSCC E protocol
486 becomes inferior to that of the CC-CV protocol after a SOC of 78 %.

487 Evolutions of relative capacity are compared on Figure 8o. The two charge protocols induce
488 a similar degradation, albeit slightly lower for MSCC E. The degradation is rather low and no
489 acceleration of capacity fade can be observed for both conditions. Cells cycled with the CC-CV
490 reference reached end-of-life between 900 and 1000 cycles, while cells cycled with MSCC E
491 lost around 28 % of their capacity after 1200 cycles. Both results show that the studied cell is
492 less impacted by fast charging at elevated temperature. Moreover, results of cycling with MSCC
493 E show that it is possible to charge at significantly higher current rates than with CC-CV for a
494 significant portion of the charge without an increase in the degradation.

495 *4.6. Discussions*

496 The experimental results call for discussions on two different topics: the proposed method to
497 optimized fast charging, specifically, and the impact of fast charging on aging, generally.

498 *4.6.1. Proposed method to define fast charging protocols*

499 The main objective of this study was to present new experimental evidence on the possibility
500 to define fast charging protocols, that do not increase aging, with numerical optimization meth-
501 ods. To that end, we used a coupled electro-thermal cell model and proposed an optimization
502 problem with several improvements, to then launch an experimental aging study with optimized
503 fast charging protocols and CC-CV protocols of comparable charge durations and capacities as
504 references.

505 Results of our experimental study demonstrated that the optimized protocols allowed to re-
506 duce charge duration and/or degradation. These results were obtained by employing a frequently
507 used electro-thermal model framework, at the cell level, and without employing an aging model.
508 Instead, aging was taken into account in an implicit manner with simple principles. Firstly, a
509 MSCC protocol is used with a sufficient number of steps to adapt the current during charge and
510 also with increasing voltage thresholds to progressively reach the upper cell voltage. Secondly,
511 a penalty is imposed on high overvoltages when charging on the last graphite phase transition.
512 Thirdly, several reasonable and compatible constraints are set on charge duration, final SOC, tem-
513 perature, current bounds, and on decreasing currents. This way of proceeding allows to quickly
514 define fast charging protocols for many operating conditions and at a low experimental cost.

515 The obtained aging results are encouraging for the method. For example, using protocol
516 MSCC A instead of the CC-CV reference protocol more than doubled the cell lifespan (Fig-
517 ure 8a). They could further be improved by enhancing the cell model or the optimization prob-
518 lem. Possible enhancements include the addition of an aging model, the optimization of voltage
519 thresholds or the adaptation of the fast charging protocols parameters to significant change in the
520 cell SOH.

521 4.6.2. Impact of fast charging on cell aging

522 Aging has to be carefully considered to enable fast charging because high currents are known
523 to accelerate several aging mechanisms. Although the optimized protocols of our experimental
524 study were successful in reducing the degradation compared to the CC-CV references, several
525 of these protocols still caused a rather rapid aging, leading to end-of-life in a few hundreds of
526 cycles. This is coherent to the findings of Sieg *et al* on another high energy cell [20]. Even
527 when seeking to charge while avoiding a prominent degradation mechanism such as lithium
528 plating, they found that high currents still caused an important degradation. Therefore, there
529 is a reasonable compromise to be made between low charge duration and high durability. For
530 example, Spingler *et al* obtained a drastic improvement in cycle life with an optimized protocol
531 compared to a CC-CV protocol of similar charging time, by allowing for a slightly longer charge
532 time or 75 min [21].

533 While a trade-off has to be made, our experimental findings nevertheless show that there ex-
534 ist opportunities for higher currents without necessarily reducing cycle life, at least for the high
535 energy NMC/G cell investigated here. One opportunity is to use high currents at low SOC, such
536 as demonstrated by case MSCC B. Indeed, currents more than two times of the recommended
537 maximum current can be used for a significant portion of the charge while still lowering degra-
538 dation compared to the CC-CV reference (Figure 8e and Figure 8f). Another opportunity is to
539 use high currents until a partial state-of-charge or lower end-of-charge voltage, such as shown
540 by case MSCC C (Figure 8h and Figure 8i), and results of Mussa *et al* [47]. Finally, there is an-
541 other opportunity for fast charging at elevated temperature such as demonstrated by case MSCC
542 E (Figure 8n and Figure 8o). These opportunities are further corroborated with the results or
543 Yang *et al* [48], that showed a very high cycle life for a high energy cell by performing a partial
544 fast-charge at elevated temperature and the discharge at a lower temperature.

545 Therefore, the results suggest the possibility to significantly reduce charging time while still

546 maintaining a good durability by using these strategies.

547 **5. Conclusions**

548 This article proposed a method to define the parameters of battery fast charging protocols by
549 numerical optimization and investigated their impact on durability.

550 A multi-stage of constant current protocol was chosen because of its straightforward frame-
551 work and its possibility to adapt the current on different state-of-charge ranges. An electro-
552 thermal model at the cell level was set up to accurately represent the cell dynamics during fast-
553 charge at different temperatures. Based on this model, a constrained optimization problem was
554 formulated. Differently from the literature, this problem considers aging in an implicit manner,
555 in the different costs and constraints. The costs penalized high currents both when the electrical
556 resistance is high, such as at low state-of-charge or low temperature, and when completing the
557 last graphite transition to the fully lithiated stage, at elevated states-of-charge. Then, charging
558 time was considered as a constraint that effectively requires high enough currents to reach the
559 target. The charging time target was further balanced by constraints on charged capacity, temper-
560 ature, current bounds, and on the decreasing of current during charge with the aim of managing
561 degradation.

562 The proposed optimization method was then used for an experimental aging study, performed
563 on a high energy lithium-ion cell with a $\text{LiNi}_{0.8}\text{Mn}_{0.1}\text{Co}_{0.1}\text{O}_2$ positive electrode and a graphite-
564 silicon oxide negative electrode. Five case studies of optimized multi-stage of constant current
565 protocols were defined by modifying three parameters: the ambient temperature, the charge time
566 constraint, and the charged capacity constraint. These protocols were compared to fast charg-
567 ing constant current-constant voltage protocols as references. The results showed that optimized
568 protocols can either improve the cell cycle life in a similar charging time, sometimes by more
569 than two-fold, or decrease the charge time without increasing the degradation. It was also ob-
570 served that there exist opportunities for significantly higher currents at low state-of-charge, with
571 a partial charge, and at elevated temperature.

572 These results suggest that the proposed optimization method can be used to define fast charg-
573 ing protocols with a lower impact on cycle life. Moreover, charge time can be further reduced
574 while maintaining a good cycle life by using the discussed strategies.

575 **Glossary**

576	SEI	solid electrolyte interphase
577	SOC	state-of-charge
578	SOH	state-of-health
579	CC-CV	constant current-constant voltage
580	MSCC	multi-stage of constant-current
581	CC	constant-current
582	CV	constant-voltage
583	NMC	lithium nickel manganese cobalt oxide
584	G	graphite
585	SiO	silicon oxide
586		

589 **Acknowledgements**

590 This work received funding from the French National Association for Technological Re-
591 search (ANRT) under grant CIFRE N° 2016/1200. The funding source had no involvement in
592 any aspect of the study or report.

593 **References**

- 594 [1] Till Bunsen, P. Cazzola, L. D'Amore, M. Gomer, S. Scheffer, R. Schuitmaker, H. Signollet, J. Tattini, J. T. L. Paoli,
595 Global EV Outlook 2019 to electric mobility, Tech. rep., International Energy Agency (2019).
- 596 [2] S. Ahmed, I. Bloom, A. N. Jansen, T. Tanim, E. J. Dufek, A. Pesaran, A. Burnham, R. B. Carlson, F. Dias, K. Hardy,
597 M. Keyser, C. Kreuzer, A. Markel, A. Meintz, C. Michelbacher, M. Mohanpurkar, P. A. Nelson, D. C. Robertson,
598 D. Scofield, M. Shirk, T. Stephens, R. Vijayagopal, J. Zhang, Enabling fast charging – A battery technology gap
599 assessment, *Journal of Power Sources* 367 (2017) 250–262. doi:10.1016/j.jpowsour.2017.06.055.
- 600 [3] M. Keyser, A. Pesaran, Q. Li, S. Santhanagopalan, K. Smith, E. Wood, S. Ahmed, I. Bloom, E. Dufek, M. Shirk,
601 A. Meintz, C. Kreuzer, C. Michelbacher, A. Burnham, T. Stephens, J. Francfort, B. Carlson, J. Zhang, R. Vi-
602 jayagopal, K. Hardy, F. Dias, M. Mohanpurkar, D. Scofield, A. N. Jansen, T. Tanim, A. Markel, Enabling fast

- 603 charging – Battery thermal considerations, *Journal of Power Sources* 367 (2017) 228–236. doi:10.1016/j.
604 jpowersour.2017.07.009.
- 605 [4] M. Abdel-Monem, K. Trad, N. Omar, OmarHegazy, B. Mantels, G. Mulder, P. V.-d. Bossche, Joeri Van Mierlo,
606 Lithium-ion batteries: Evaluation study of different charging methodologies based on aging process, *Applied Energy*
607 152. doi:10.1016/j.apenergy.2015.02.064.
- 608 [5] P. Keil, A. Jossen, Charging protocols for lithium-ion batteries and their impact on cycle life-An experimental
609 study with different 18650 high-power cells, *Journal of Energy Storage* 6 (2016) 125–141. doi:10.1016/j.est.
610 2016.02.005.
- 611 [6] S. S. Zhang, The effect of the charging protocol on the cycle life of a Li-ion battery, *Journal of Power Sources*
612 161 (June) (2006) 1385–1391. doi:10.1016/j.jpowersour.2006.06.040.
- 613 [7] N. Omar, M. A. Monem, Y. Firouz, J. Salminen, J. Smekens, O. Hegazy, H. Gaulous, G. Mulder, P. Van den
614 Bossche, T. Coosemans, J. Van Mierlo, Lithium iron phosphate based battery - Assessment of the aging parameters
615 and development of cycle life model, *Applied Energy* 113 (2014) 1575–1585. doi:10.1016/j.apenergy.2013.
616 09.003.
- 617 [8] T. Waldmann, B. I. Hogg, M. Wohlfahrt-Mehrens, Li plating as unwanted side reaction in commercial Li-ion cells –
618 A review, *Journal of Power Sources* 384 (February) (2018) 107–124. doi:10.1016/j.jpowersour.2018.02.063.
- 619 [9] S. J. An, J. Li, C. Daniel, D. Mohanty, S. Nagpure, D. L. Wood, The state of understanding of the lithium-ion-
620 battery graphite solid electrolyte interphase (SEI) and its relationship to formation cycling, *Carbon* 105 (2016)
621 52–76. doi:10.1016/j.carbon.2016.04.008.
- 622 [10] I. Laresgoiti, S. Käbitz, M. Ecker, D. U. Sauer, Modeling mechanical degradation in lithium ion batteries during
623 cycling : Solid electrolyte interphase fracture, *Journal of Power Sources* 300 (2015) 112–122. doi:10.1016/j.
624 jpowersour.2015.09.033.
- 625 [11] S. Zhang, Chemomechanical modeling of lithiation-induced failure in high-volume-change electrode materials for
626 lithium ion batteries, *npj Computational Materials* 3 (1) (2017) 1–11. doi:10.1038/s41524-017-0009-z.
- 627 [12] X. Fleury, M. H. Noh, S. Geniès, P. X. Thivel, C. Lefrou, Y. Bultel, Fast-charging of Lithium Iron Phosphate
628 battery with ohmic-drop compensation method: Ageing study, *Journal of Energy Storage* 16 (2018) 21–36. doi:
629 10.1016/j.est.2017.12.015.
- 630 [13] M. Abdel-Monem, K. Trad, N. Omar, O. Hegazy, P. Van den Bossche, J. Van Mierlo, Influence analysis of static
631 and dynamic fast-charging current profiles on ageing performance of commercial lithium-ion batteries, *Energy*
632 120 (2017) (2017) 179–191. doi:10.1016/j.energy.2016.12.110.
- 633 [14] C. Zhang, J. Jiang, Y. Gao, W. Zhang, Q. Liu, X. Hu, Charging optimization in lithium-ion batteries based on
634 temperature rise and charge time, *Applied Energy* 194 (2017) 569–577. doi:10.1016/j.apenergy.2016.10.
635 059.
- 636 [15] S. Schindler, M. Bauer, H. Cheetamun, M. A. Danzer, Fast charging of lithium-ion cells: Identification of aging-
637 minimal current profiles using a design of experiment approach and a mechanistic degradation analysis, *Journal of*
638 *Energy Storage* 19 (March) (2018) 364–378. doi:10.1016/j.est.2018.08.002.
- 639 [16] Z. Guo, B. Yann, X. Qiu, L. Gao, C. Zhang, Optimal charging method for lithium ion batteries using a univer-
640 sal voltage protocol accommodating aging, *Journal of Power Sources* 274 (2015) 957–964. doi:10.1016/j.
641 jpowersour.2014.10.185.

- 642 [17] H. E. Perez, X. Hu, S. Dey, S. J. Moura, Optimal Charging of Li-Ion Batteries with Coupled Electro-Thermal-
643 Aging Dynamics, *IEEE Transactions on Vehicular Technology* 66 (9) (2017) 7761–7770. doi:10.1109/TVT.
644 2017.2676044.
- 645 [18] T. Waldmann, M. Kasper, M. Wohlfahrt-Mehrens, Optimization of Charging Strategy by Prevention of Lithium
646 Deposition on Anodes in high-energy Lithium-ion Batteries - Electrochemical Experiments, *Electrochimica Acta*
647 178 (2015) 525–532. doi:10.1016/j.electacta.2015.08.056.
- 648 [19] T. Amietszajew, E. McTurk, J. Fleming, R. Bhagat, Understanding the limits of rapid charging using instru-
649 mented commercial 18650 high-energy Li-ion cells, *Electrochimica Acta* 263 (2018) 346–352. doi:10.1016/
650 j.electacta.2018.01.076.
- 651 [20] J. Sieg, J. Bandlow, T. Mitsch, D. Dragicevic, T. Materna, B. Spier, H. Witzhausen, M. Ecker, D. U. Sauer, Fast
652 charging of an electric vehicle lithium-ion battery at the limit of the lithium deposition process, *Journal of Power*
653 *Sources* 427 (2019) 260–270. doi:10.1016/j.jpowsour.2019.226846.
- 654 [21] F. B. Spingler, W. Wittmann, J. Sturm, B. Rieger, A. Jossen, Optimum fast charging of lithium-ion pouch cells
655 based on local volume expansion criteria, *Journal of Power Sources* 393 (February) (2018) 152–160. doi:10.
656 1016/j.jpowsour.2018.04.095.
- 657 [22] U. R. Koleti, C. Zhang, R. Malik, T. Q. Dinh, J. Marco, The development of optimal charging strategies for
658 lithium-ion batteries to prevent the onset of lithium plating at low ambient temperatures, *Journal of Energy Storage*
659 24 (June). doi:10.1016/j.est.2019.100798.
- 660 [23] Y. H. Liu, C. H. Hsieh, Y. F. Luo, Search for an optimal five-step charging pattern for li-ion batteries us-
661 ing consecutive orthogonal arrays, *IEEE Transactions on Energy Conversion* 26 (2) (2011) 654–661. doi:
662 10.1109/TEC.2010.2103077.
- 663 [24] T. T. Vo, X. Chen, W. Shen, A. Kapoor, New charging strategy for lithium-ion batteries based on the integration of
664 Taguchi method and state of charge estimation, *Journal of Power Sources* 273 (2015) 413–422. doi:10.1016/j.
665 jpowsour.2014.09.108.
- 666 [25] A. Abdollahi, X. Han, N. Raghunathan, B. Pattipati, B. Balasingam, K. Pattipati, Y. Bar-Shalom, B. Card, Optimal
667 charging for general equivalent electrical battery model, and battery life management, *Journal of Energy Storage* 9
668 (2017) 47–58. doi:10.1016/j.est.2016.11.002.
- 669 [26] K. Liu, K. Li, Z. Yang, C. Zhang, J. Deng, Battery optimal charging strategy based on a coupled thermoelectric
670 model, *Electrochimica Acta* 225 (2017) 330–344. doi:10.1109/CEC.2016.7748334.
- 671 [27] R. Suresh, R. Rengaswamy, Modeling and control of battery systems. Part II: A model predictive controller for
672 optimal charging, *Computers and Chemical Engineering* 119 (2018) 326–335. doi:10.1016/j.compchemeng.
673 2018.08.017.
- 674 [28] X. Lin, X. Hao, Z. Liu, W. Jia, Health conscious fast charging of Li-ion batteries via a single particle model with
675 aging mechanisms, *Journal of Power Sources* 400 (May) (2018) 305–316. doi:10.1016/j.jpowsour.2018.
676 08.030.
- 677 [29] M. R. Palacín, Understanding ageing in Li-ion batteries: A chemical issue, *Chemical Society Reviews* 47 (13)
678 (2018) 4924–4933. doi:10.1039/c7cs00889a.
- 679 [30] X. G. Yang, C. Y. Wang, Understanding the trilemma of fast charging, energy density and cycle life of lithium-ion
680 batteries, *Journal of Power Sources* 402 (September) (2018) 489–498. doi:10.1016/j.jpowsour.2018.09.

- 681 069.
- 682 [31] R. Mathieu, O. Briat, P. Gyan, J.-M. Vinassa, Comparison of the impact of fast charging on the cycle life of
683 three lithium-ion cells under several parameters of charge protocol and temperatures, *Applied Energy* 283. doi:
684 10.1016/j.apenergy.2020.116344.
- 685 [32] R. Mathieu, O. Briat, P. Gyan, J.-M. Vinassa, Electro-thermal behavior of four fast charging protocols for a lithium-
686 ion cell at different temperatures, in: *Proceedings: IECON 2018 - 44th Annual Conference of the IEEE Industrial*
687 *Electronics Society, IEEE*, 2018. doi:10.1109/IECON.2018.8591603.
- 688 [33] X. Lin, H. E. Perez, S. Mohan, J. B. Siegel, A. G. Stefanopoulou, Y. Ding, M. P. Castanier, A lumped-parameter
689 electro-thermal model for cylindrical batteries, *Journal of Power Sources* 257 (2014) 1–11. doi:10.1016/j.
690 jpowersour.2014.01.097.
- 691 [34] N. Damay, C. Forgez, M.-p. Bichat, G. Friedrich, Thermal modeling of large prismatic LiFePO₄ / graphite battery
692 . Coupled thermal and heat generation models for characterization and simulation, *Journal of Power Sources* 283
693 (2015) 37–45. doi:10.1016/j.jpowersour.2015.02.091.
- 694 [35] Y. C. Zhang, O. Briat, L. Boulon, J. Y. Deletage, C. Martin, F. Coccetti, J. M. Vinassa, Non-isothermal Ragone
695 plots of Li-ion cells from datasheet and galvanostatic discharge tests, *Applied Energy* 247 (2019) 703–715. doi:
696 10.1016/j.apenergy.2019.04.027.
- 697 [36] A. Farmann, D. U. Sauer, Comparative study of reduced order equivalent circuit models for on-board state-of-
698 available-power prediction of lithium-ion batteries in electric vehicles, *Applied Energy* 225 (April) (2018) 1102–
699 1122. doi:10.1016/j.apenergy.2018.05.066.
- 700 [37] C. R. Birkel, E. McTurk, M. R. Roberts, P. G. Bruce, D. A. Howey, A Parametric Open Circuit Voltage Model for
701 Lithium Ion Batteries, *Journal of The Electrochemical Society* 162 (12) (2015) A2271–A2280. doi:10.1149/2.
702 0331512jes.
- 703 [38] C. Forgez, D. Vinh Do, G. Friedrich, M. Morcrette, C. Delacourt, Thermal modeling of a cylindrical
704 LiFePO₄/graphite lithium-ion battery, *Journal of Power Sources* 195 (9) (2010) 2961–2968. doi:10.1016/j.
705 jpowersour.2009.10.105.
- 706 [39] K. E. Thomas, J. Newman, Heats of mixing and of entropy in porous insertion electrodes, *Journal of Power Sources*
707 119-121 (2003) 844–849. doi:10.1016/S0378-7753(03)00283-0.
- 708 [40] J. Nocedal, S. J. Wright, *Numerical Optimization*, Springer, New York, 2006. doi:https://doi.org/10.1007/
709 978-0-387-40065-5.
- 710 [41] M. Dubarry, C. Truchot, B. Y. Liaw, Synthesize battery degradation modes via a diagnostic and prognostic model,
711 *Journal of Power Sources* 219 (2012) 204–216. doi:10.1016/j.jpowersour.2012.07.016.
- 712 [42] M. Heß, Kinetics and stage transitions of graphite for lithium-ion batteries, Ph.D. thesis, Swiss Federal Institute of
713 Technology of Zurich (2013). doi:10.3929/ethz-a-010000442.
- 714 [43] T. T. D. Nguyen, S. Abada, A. Lecocq, J. Bernard, M. Petit, G. Marlair, S. Grugeon, S. Laruelle, Under-
715 standing the thermal runaway of ni-rich lithium-ion batteries, *World Electric Vehicle Journal* 10 (4). doi:
716 10.3390/wevj10040079.
- 717 [44] S. F. Schuster, T. Bach, E. Fleder, J. Müller, M. Brand, G. SEXTL, A. Jossen, Nonlinear aging characteristics of
718 lithium-ion cells under different operational conditions, *Journal of Energy Storage* 1 (1) (2015) 44–53. doi:
719 10.1016/j.est.2015.05.003.

- 720 [45] M. Dubarry, G. Baure, D. Anseán, Perspective on State-of-Health Determination in Lithium-Ion Batteries, *Journal*
721 *of Electrochemical Energy Conversion and Storage* 17 (4). doi:10.1115/1.4045008.
- 722 [46] J. Wang, J. Purewal, J. Graetz, S. Soukiazian, H. Tataria, M. W. Verbrugge, Degradation of lithium ion batteries
723 employing graphite negatives and nickel-cobalt-manganese oxide + spinel manganese oxide positives: Part 2,
724 chemical-mechanical degradation model, *Journal of Power Sources* 272 (2014) 1154–1161. doi:10.1016/j.
725 jpowsour.2014.07.028.
- 726 [47] A. S. Mussa, M. Klett, M. Behm, G. Lindbergh, R. W. Lindström, Fast-charging to a partial state of charge in
727 lithium-ion batteries: A comparative ageing study, *Journal of Energy Storage* 13 (2017) 325–333. doi:10.1016/
728 j.est.2017.07.004.
- 729 [48] X.-g. Yang, T. Liu, S. Ge, Y. Leng, D. Wang, X.-g. Yang, T. Liu, Y. Gao, S. Ge, Y. Leng, D. Wang, Asymmetric
730 Temperature Modulation for Extreme Fast Charging of Lithium-Ion Batteries Asymmetric Temperature Modulation
731 for Extreme Fast Charging of Lithium-Ion Batteries, *Joule* 3 (2019) 1–18. doi:10.1016/j.joule.2019.09.
732 021.